



HAL
open science

PbS quantum dot thin film dry etching

Nicolas Le Brun, Gilles Cunge, Pascal Gouraud, Camille Petit-Etienne, Linda Parmigiani, Stéphane Allegret-Maret, Denis Guiheux, Jonathan Steckel

► **To cite this version:**

Nicolas Le Brun, Gilles Cunge, Pascal Gouraud, Camille Petit-Etienne, Linda Parmigiani, et al.. PbS quantum dot thin film dry etching. *Journal of Vacuum Science & Technology A*, 2024, 42 (3), 10.1116/6.0003335 . hal-04777187

HAL Id: hal-04777187

<https://hal.science/hal-04777187v1>






Submitted on 12 Nov 2024

HAL is a multi-disciplinary open access archive for the deposit and dissemination of scientific research documents, whether they are published or not. The documents may come from teaching and research institutions in France or abroad, or from public or private research centers.

L'archive ouverte pluridisciplinaire **HAL**, est destinée au dépôt et à la diffusion de documents scientifiques de niveau recherche, publiés ou non, émanant des établissements d'enseignement et de recherche français ou étrangers, des laboratoires publics ou privés.

RESEARCH ARTICLE | APRIL 08 2024

PbS quantum dot thin film dry etching

Nicolas Le Brun ; Gilles Cunge ; Pascal Gouraud ; Camille Petit-Etienne ; Linda Parmigiani; Stéphane Allegret-Maret; Denis Guiheux; Jonathan S. Steckel 



J. Vac. Sci. Technol. A 42, 033007 (2024)

<https://doi.org/10.1116/6.0003335>



Articles You May Be Interested In

Highly sensitive SWIR photodetector using carbon nanotube thin film transistor gated by quantum dots heterojunction

Appl. Phys. Lett. (May 2022)

Room-temperature nanostructured PbSe/CdSe mid-infrared photodetector: Annealing effects

J. Vac. Sci. Technol. B (January 2024)



Instruments for Advanced Science



- Knowledge
- Experience
- Expertise

[Click to view our product catalogue](#)

Contact Hiden Analytical for further details:

www.HidenAnalytical.com
 info@hiden.co.uk



Gas Analysis

- ▶ dynamic measurement of reaction gas streams
- ▶ catalysis and thermal analysis
- ▶ molecular beam studies
- ▶ dissolved species probes
- ▶ fermentation, environmental and ecological studies



Surface Science

- ▶ UHV TPD
- ▶ SIMS
- ▶ end point detection in ion beam etch
- ▶ elemental imaging - surface mapping



Plasma Diagnostics

- ▶ plasma source characterization
- ▶ etch and deposition process reaction kinetic studies
- ▶ analysis of neutral and radical species



Vacuum Analysis

- ▶ partial pressure measurement and control of process gases
- ▶ reactive sputter process control
- ▶ vacuum diagnostics
- ▶ vacuum coating process monitoring

PbS quantum dot thin film dry etching



Cite as: J. Vac. Sci. Technol. A 42, 033007 (2024); doi: 10.1116/6.0003335

Submitted: 29 November 2023 · Accepted: 12 March 2024 ·

Published Online: 8 April 2024



Nicolas Le Brun,^{1,2,a)} Gilles Cunge,¹ Pascal Gouraud,² Camille Petit-Etienne,¹ Linda Parmigiani,² Stéphane Allegret-Maret,² Denis Guiheux,² and Jonathan S. Steckel²

AFFILIATIONS

¹Institute of Engineering and Management University Grenoble Alpes, LTM, University Grenoble Alpes, CNRS, CEA/LETI-Minatec, Grenoble INP, Grenoble F-38054, France

²STMicroelectronics, Montrouge 92120, France

^{a)}Author to whom correspondence should be addressed: nlb2208@gmail.com

ABSTRACT

Many consumer products used daily contain sensors and image sensors (smartphones, cars, automated tools, etc.). There is a growing demand to enhance the capabilities of industrial products to probe their environment more efficiently, i.e., under difficult conditions (smoke, darkness, etc.). One solution is to extend the capabilities of image sensors to detect light toward the near-infrared and short-wave infrared (SWIR) regions. Because silicon has weak absorption properties in the infrared, especially in the SWIR region, manufacturers are investigating the use of new materials to build these sensors. To this end, colloidal quantum dot (QD) thin films made from the assembly of PbS nanoparticles have emerged as promising materials. They offer tunable bandgaps, favorable absorption properties, and scalability in production. However, patterning the active parts of photodiodes by plasma etching of this new material presents challenges. The etching chemistry must be selected to volatilize Pb and S without modifying the unetched active part of the PbS QD photodiode, and the etching profile should be anisotropic. In this study, we have screened several plasma operating conditions (power, pressure, and temperature) in various chemistries (H₂, Cl₂, HBr, and N₂). To understand the etch mechanisms and profiles, ToF-SIMS and TEM/energy dispersive x-ray were employed. Our findings reveal that halogen-based plasmas cause QD material deterioration through Cl or Br diffusion deep in the film. While H₂ plasmas are efficient to etch PbS QD films, they result in high roughness due to the removal of the carbonated ligands that separate PbS QDs. This ligand etching is followed by QD coalescence leading to significant roughness. However, the addition of N₂ to H₂ can prevent this phenomenon by forming a diffusion barrier at the surface, resulting in favorable etching characteristics.

Published under an exclusive license by the AVS. <https://doi.org/10.1116/6.0003335>

I. INTRODUCTION

Several manufacturers across various industries are working diligently to improve the efficiency of light detection sensors and devices. The surge in demand motivates semiconductor manufacturers to develop new sensing technologies that can enable both mass volume production and high efficiency imaging in diverse conditions, such as challenging environments like fog, smoke, water, and darkness. Recently, focus has emerged on infrared (IR) wavelengths to bypass some limitations of visible complementary metal-oxide-semiconductor (CMOS) image sensors, opening new possible applications.¹ Since the solar spectrum has a very low intensity at specific wavelength (due to light absorption in the atmosphere, for example, at 1.11 and 1.4 μm as shown in Fig. 1), designing a sensor to detect light at these wavelengths offers the advantage of ultralow background noise, allowing it to fully use IR detection properties.

However, the industry faces a serious challenge in detecting IR wavelengths. Silicon, the predominant material for visible light detection, is transparent³ to wavelengths above 1.1 μm. Consequently, a crucial challenge lies in identifying a detector material capable of absorbing light within specific wavelengths ranging from near-infrared (NIR) to short-wave infrared (SWIR). This material must also be compatible with CMOS fabrication technologies.

A promising material to meet these requirements is the Quantum Dot (QD) thin film technology, that we refer to as quantum film or QF.⁴ QF consists of the solution assembly of semiconductor QDs, creating a photoactive layer capable of absorbing IR light.

The tunable size of QD, ranging from approximately 2 to 10 nm, allows for the adjustment of the film bandgap, determining the optimal absorbing wavelength. Based on the size and shape of

12 November 2024 14:43:05

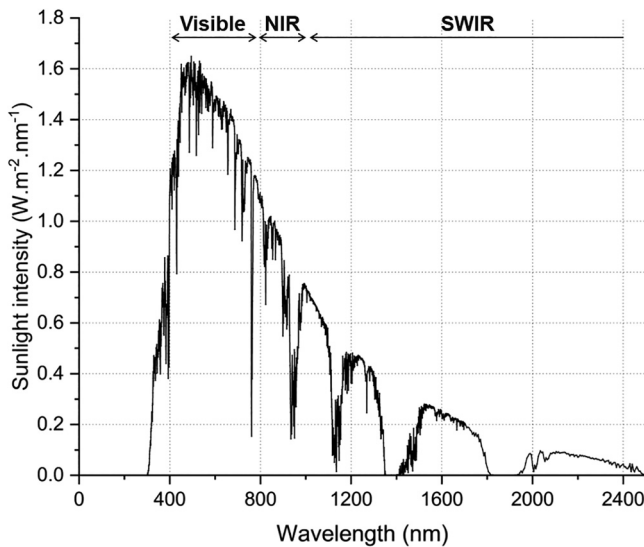


FIG. 1. AM1.5 (Air Mass 1.5 standard) solar irradiance spectrum. Atmospheric absorption is included (Ref. 2). Visible, NIR, and SWIR regions are defined.

the QDs, the excited state becomes quantum confined, leading to discrete energy states with a bandgap that decreases as the QD size increases. This inherent property positions QF as a promising material to build IR sensors.

Various methods and materials can be used to obtain QF.^{5,6} In this paper, we used lead sulfide (PbS) nanocrystals grown in a colloidal solution and subsequently deposited on 300 mm diameter wafers through a spin-coating process. The resulting film is then passivated and stabilized, giving it the desired properties. A schematic of a PbS QF is described in Fig. 2. As it is represented, PbS QDs are bonded together by organic ligands, and there are inorganic passivators incorporated into the film to stabilize it.

QF technology allows for repeatable and low-cost manufacturing techniques, positioning it as a highly promising technology for producing sensors on a large-scale. However, after the QF deposition, there are several critical manufacturing steps that must be optimized to successfully manage the fabrication of a functional IR

optical sensor. Notably, patterning the photodiode constitutes a significant challenge. The patterning follows a typical top-down approach starting by deposition of a multilayer hard mask. This hard mask serves multiple purposes, including encapsulating the QF to prevent oxidation, acting as a waveguide, and ensuring sufficient selectivity during plasma etching. Subsequently, photolithography is used to pattern a resist mask on top of the hard mask. Multiple plasma etching steps are then executed to transfer the resist mask into the hard mask and finally to pattern QF active layer through the resist/hard mask. This work is focused on the dry etching of the PbS QD thin film under various plasma operating conditions and chemistries. Understanding plasma interactions with this material is essential to ensure creation of volatile species and maintain control over the process.

Plasma etching mechanisms of PbS QF are poorly documented in the literature. A few papers refer to etching PbS QD films using $\text{CH}_4/\text{H}_2/\text{Ar}$ plasma, i.e., typical etching chemistry for II/VI semiconductors.⁷⁻⁹

It is, thus, important to analyze the etching mechanisms of PbS QF in various plasma chemistries. Since the QF is very sensitive to oxygen and the film stability requires etching at low temperature ($<120^\circ\text{C}$), our focus is on the PbS QD etching mechanisms in high density Cl_2 , HBr, CF_4 , H_2 , and N_2/H_2 plasma chemistries.

II. EXPERIMENTAL SETUP

Experiments are conducted in a Lam inductively coupled plasma (ICP) Kiyoo reactor, accepting 300 mm diameter wafers. The electrostatic chuck temperature was maintained in the range of 10–120 °C throughout all experiments using a helium backside conditioning flow. The plasma was operated within pressures and RF power ranges of 2–40 m Torr and 500–2000 W, respectively, while bias voltage was applied in the 0–700 V range. For partial etching of the QF film, we employed a fixed timed etch, preserving approximately 20%–50% of the initial thickness. A schematic of the partial etched profile is represented in Fig. 3.

By using several surface analysis techniques, we analyzed the remaining QF film directly after plasma exposure, giving us insights into the plasma etching mechanism in different chemistries. Initial observations of the resulting profile were made using scanning electron microscopy (SEM) through an Applied Material SEMVision tool, allowing tilting of the wafer for angled pattern observations. Cross-sectional SEM measurements were conducted using a

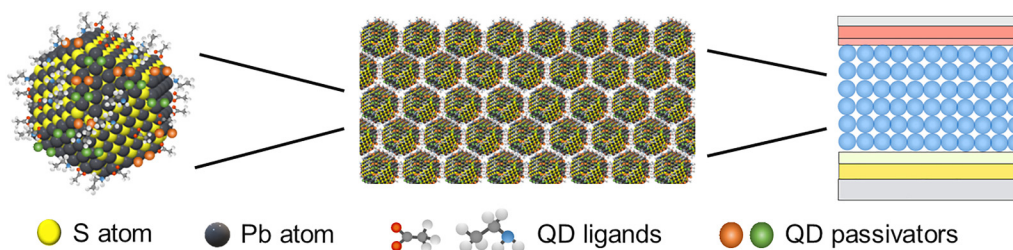


FIG. 2. Schematic representation of a PbS QD, quantum dot close-packed thin film, and an optical sensor device architecture.

12 November 2024 14:43:05

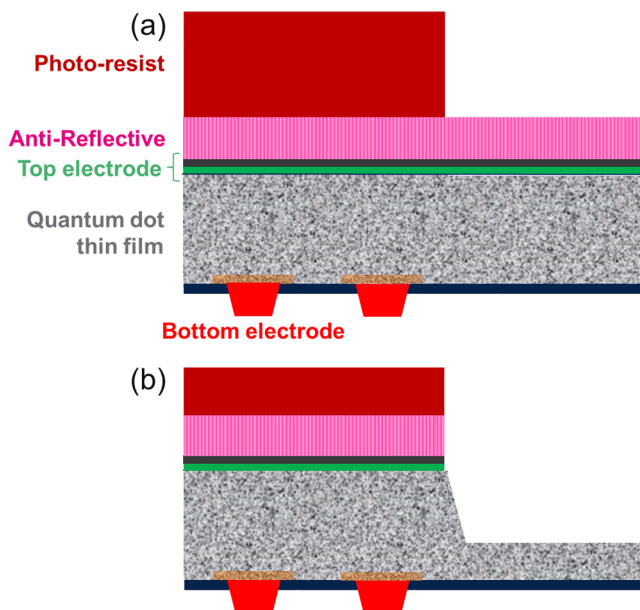


FIG. 3. Schematic of the partially etched QD device stack. (a) Before etching and (b) after partial etching.

Hitachi 4800 tool. Transmission electron microscopy (TEM) analysis combined by an energy dispersive x-ray (EDX) spectroscopy measurement was then performed to analyze the thickness and chemical composition of the passivation layer which forms on the feature sidewalls (as well as on the reactive layer which drives the etching at the feature bottom). TEM and EDX analysis were carried out using a Thermo Fisher Osiris tool. Since some atoms could not be detected by EDX measurements (hydrogen), secondary ion mass spectrometry coupled with time-of-flight (ToF-SIMS) measurements have also been performed with a IONTOF GmbH ToF-SIMS 5 tool to follow the concentration of some elements through the remaining QF. Additionally, atomic force microscopy (AFM) was performed to determine the resulting surface roughness. This was achieved using a Bruker Dimension ICON tool.

III. RESULTS AND DISCUSSION

A. Etching chemistry screening

To understand the phenomenon occurring during the QF etch, we analyzed several plasma chemistries: HBr, Cl₂, CF₄, and H₂. In each case, the reactive gas was diluted in 50% Ar to enable a high total gas flow rate, facilitating the rapid removal of etch products from the plasma. The initial parameter examined was the etch rate for each chemistry, serving as a quick indicator of a plasma/surface interaction. Etch rate was calculated by dividing the thickness etched by the etching duration, as shown in Fig. 4. ICP RF power and DC bias voltage were chosen to ensure the wafer is bombarded by a significant flux of energetic ions, facilitating QF etching. It is worth noting that due to the lower ionization energy

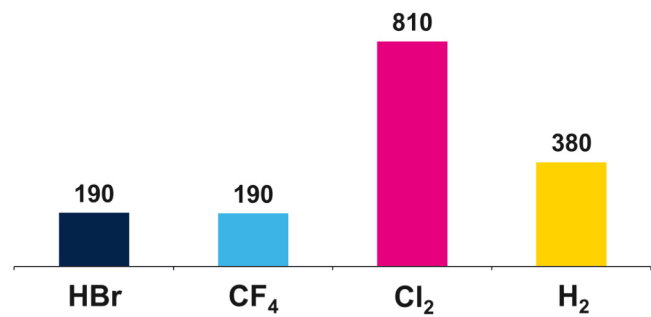


FIG. 4. Etch rates (nm min⁻¹) calculated for each etching plasma chemistries.

threshold of Pb (7.4 eV) compared to Cl_x, Br_x, H_x, and CF_x, we expected predominant ions to be Pb-based, independent of the etch chemistry. This expectation aligns with observations made during silicon etching in similar plasma.¹⁰

Figure 4 illustrates that the QF etch rates in Cl₂ and H₂ plasmas are high, suggesting that etching byproducts like PbCl_x, SCl_x, PbH_x, and SH_x are highly volatile. By contrast, chemistries based on Br and F result in a relatively slow etching of the QF film. The corresponding SEM and TEM-EDX analyses of the etch profiles are shown in Fig. 5.

Prior to discussing the etching profile, it is important to note that the etch is performed after opening a trilayer hard mask containing metallic elements. Following the plasma etching of this mask, nonvolatile metallic residues are already present, coating the sidewalls of the resist mask. This layer should not be confused with the sidewall passivation layers that form during the QF etching, as discussed below. This initial sidewall layer is particularly well visible in Fig. 5(h) after QF etching in H₂, appearing in yellow.

The QF etching profile after plasma etching in HBr chemistry shows highly tapered sidewalls, Fig. 5(a). This is attributed to the formation of a thick sidewall passivation layer, primarily composed of PbBr_x. The observed tapering indicates a predominantly physical etching mechanism, where poorly volatile PbBr_x etch products are sputtered onto the sidewalls instead of creating volatile species. This aligns with the earlier suggestion derived from the low etch rate. Moreover, Fig. 5(e) shows that bromine atoms, despite their large atomic radii, penetrated deeply beneath the mask into the QF stack during the etching step, which threatens the integrity of the final product. Consequently, HBr plasma chemistry is clearly not a favorable choice for patterning the QF film.

The etched sidewalls created during the CF₄ enhanced etching [Figs. 5(b) and 5(f)] also exhibit tapering with a thick passivation layer on both the mask and feature sidewalls. This aligns well with the slow etching rate, indicating that fluorine-based etch products of Pb and S are poorly volatile. Furthermore, the passivation layer exhibits hornlike structures at the top of the photoresist mask, suggesting poor etching selectivity between QF and photoresist. Consequently, CF₄-based plasmas are not an optimal choice of plasma chemistry for etching the QF.

Figures 5(c) and 5(g) show that QF etching in Cl₂ plasma leads to more vertical featured sidewalls due to the formation of a

12 November 2024 14:43:05

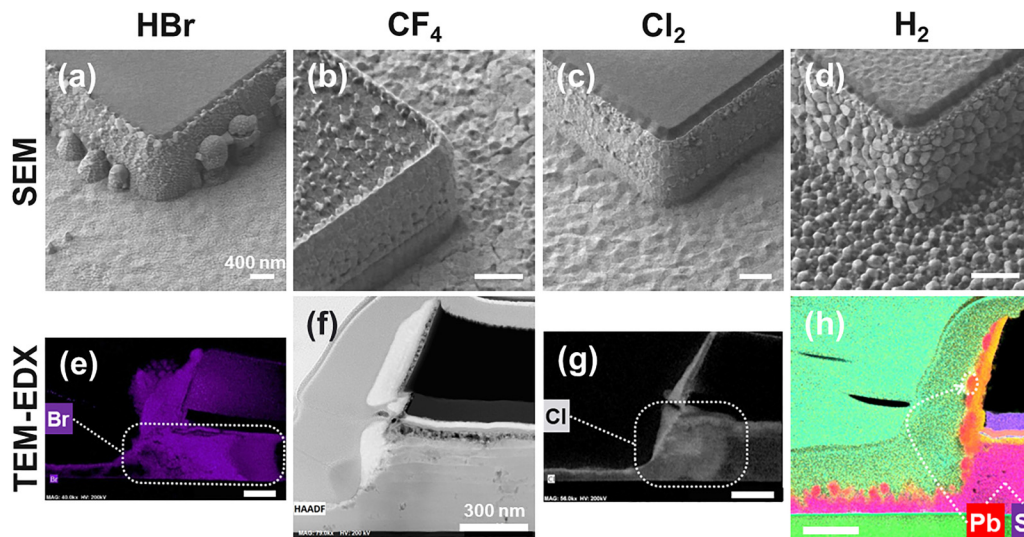


FIG. 5. Tilted SEM [(a)–(d)], TEM (f), and TEM-EDX [(e), (g), and (h)] images of resulting profiles after partial etching using (a) and (e) HBr plasma, (b) and (f) CF_4 plasma, (c) and (g) Cl_2 plasma, and (d) and (h) H_2 plasma. SEM scale bars are 400 nm [(a)–(d)]. TEM and TEM-EDX scale bars are 300 nm [(e)–(h)].

relatively thin passivation layer. Consistent with the high etch rate, suggesting the formation of highly volatile chlorinated etch product that are easily pumped out, minimizing redeposition on featured sidewalls. Furthermore, owing to the fast etch rate, the sidewalls are exposed to plasma-fragmented etch products for a shorter duration compared to HBr and CF_4 plasmas. This results in thinner passivation layers. While the etching rate and anisotropy are acceptable in Cl_2 -based plasmas, the TEM-EDX picture in Fig. 5(g) indicates lateral diffusion of Cl deep into the QF film beneath the mask. Despite the favorable morphological etching properties, the lateral diffusion of Cl (and Br) over several 100 nanometers into the film may adversely impact the optical properties of the final product. This diffusion is expected considering QF is made up of colloidal assemblies of nanoparticles, where radical diffusion is highly favored between the QDs compared to a bulk material like silicon, which are essentially impermeable to thermal Cl and Br atoms. Therefore, despite the good morphologic etching properties obtained in Cl_2 , it is not recommended for patterning the QF.

Finally, as shown in Figs. 5(d) and 5(h), the QF etching profiles obtained in H_2 chemistry are anisotropic, despite the presence of a significant roughness both on the feature sidewalls and on the etch front. The thin passivation layer suggests that the etch products are relatively volatile, aligning with the observed high etch rate. However, due to the inability to detect H atoms by EDX, it remains impossible to determine if H has diffused into the PbS QF underneath the mask. To address this, ToF-SIMS was chosen, as it is an effective method for probing the presence of hydrogen in a film and analyzing its concentration profile with depth. This method also provides valuable insights into the etching mechanism by determining the density profile of various atomic and molecular species, including S, Pb, C, CN, etc.

Figure 6 shows the depth profiling of three major elements initially present in the QF (Pb and S from the QD and CN from

the ligands) along with H atoms. It shows that the hydrogen concentration decreases constantly with the depth probed by SIMS, meaning H atoms can diffuse deep into the film during the etch step, as previously observed with halogen atoms. The results reveal surface nodes that are sulfur and CN bonds depleted while being lead and hydrogen rich. The CN bonds mostly correspond to the organic matrix of the QF, i.e., ligands surrounding each PbS quantum dot, preventing coalescence. These results suggest that hydrogen atoms preferentially create volatile species, such as H_2S and CH_x , with sulfur atoms and with the organic matrix of the film, rather than with lead atoms. The diffusion of hydrogen atoms into the film implies etching of ligands and sulfur atoms tens of nanometer deep. As sulfur, QD ligands and passivators are etched, the QF film loses stability, prompting lead particles to coalesce and form the observed nodes in SEM images. A schematic reaction model has been drawn to represent the phenomena occurring during the H_2 etch (Fig. 7).

B. Impact of the process parameters on QF etch in H_2 plasmas

To further investigate H diffusion mechanisms and explore possible mitigation strategies, we adjusted the etching process parameters. We specifically analyzed the impact of the bias voltage applied to the wafer (modifying the energy of the incident ions to the surface), the effect of the plasma pressure (expected to control the H density), and the influence of the wafer temperature (controlling H diffusion into the material). The resulting roughness, considered a reliable indicator of plasma-induced damage in the QF, was then monitored by SEM and AFM after partial etching. The results are shown in Fig. 8 and Table I.

Figure 8 and Table I shows first that there is no apparent correlation between the etch rate and the surface roughness. Lowering

12 November 2024 14:43:05

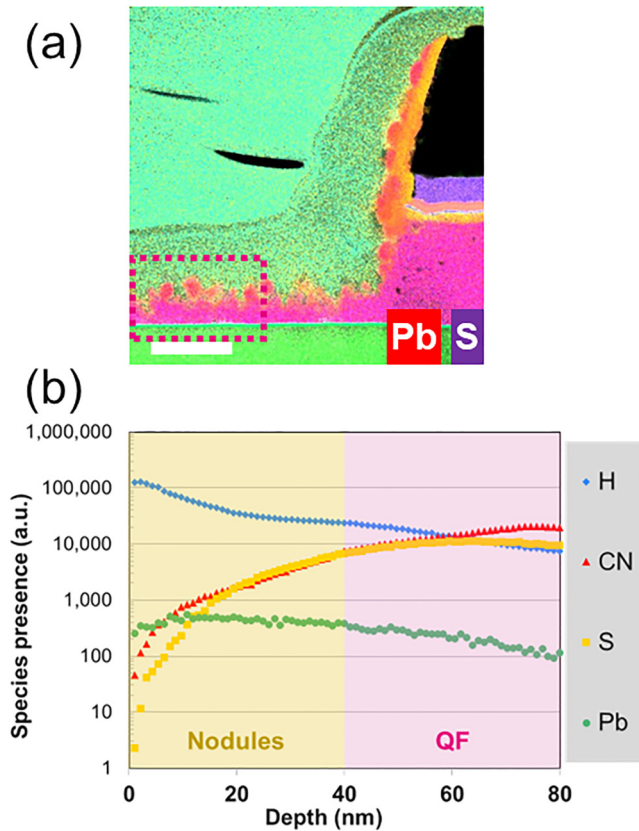


FIG. 6. ToF-SIMS analysis of the remaining quantum film after a partial H_2 etch: (a) probed area and (b) QF main elements density profiles. Scale bar is 300 nm on TEM-EDX (a) picture.

the ion energy significantly increases roughness, while reducing pressure and temperature leads to a significant reduction of surface nodes dimension. Decreasing plasma pressure reduces the H atoms flux to the wafer but also enhances ion flux (the ion flux measured without bias by a capacitively coupled ion flux probe is increasing by a factor 1.5 when the pressure is decreased under our condition).¹¹ The etch rate is weakly affected but is more ion driven, resulting in a reduced roughness since the physical sputtering of Pb is favored compared to the chemical etching of S and C-rich ligand deep in the film. By contrast, reducing the ion energy at constant ion flux and H atom flux significantly increases surface roughness. This is attributed to reduced ion enhanced etching of Pb while maintaining the same rate of etching for C ligands and S. This imbalance between the etching of lead atoms and the etching of sulfur and ligands results in a higher roughness.

Finally, lowering the wafer temperature is expected to reduce the chemical reaction rate of H with C and S, as well as decreasing the diffusion rate of H within the film. As shown in Table I, this indeed results in a significant reduction in roughness. Those observations align coherently with the proposed mechanism of roughness formation by coalescence of Pb dot fragments following the

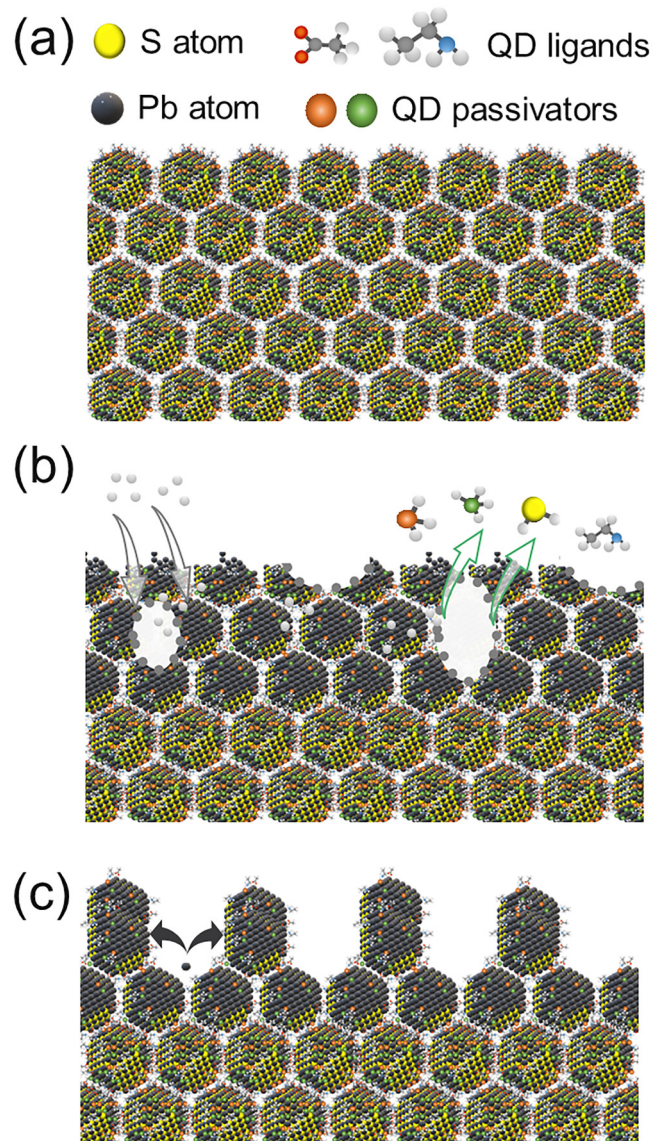


FIG. 7. Schematic reaction model of a QF H_2 plasma etch represented in three steps: (a) initial QF, (b) during, and (c) after the etching process.

chemical etching of ligand and S by H atoms, while Pb etching is more ion assisted.

This experiment shows that reducing plasma pressure and wafer temperature can effectively reduce node size. However, even with the modification of these process parameters, residual nodes persist at the surface, meaning the etch front is not uniform and hydrogen atoms still diffuse into the stack. The addition of a “passivating” gas into H_2 remains the last option to form a diffusion barrier that minimizes H diffusion in the bulk QF.

12 November 2024 14:43:05

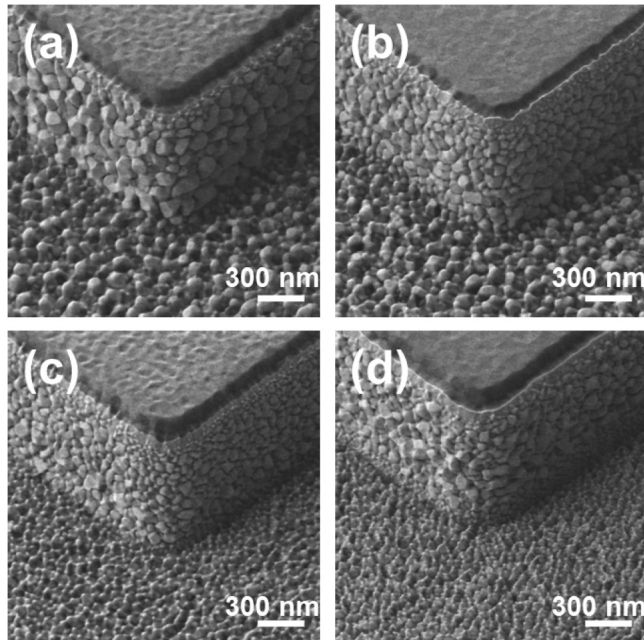


FIG. 8. SEM pictures indicating process parameters effects on resulting etching profiles, screened from a H₂ plasma partial etch; (a) reference; (b) low bias voltage; (c) low plasma pressure; and (d) low wafer temperature. All scale bars are 300 nm.

C. H₂ etch using additional chemistries

Additions of 10% and 15% CH₄ and N₂ to the H₂-based plasma were investigated. The resulting etching profiles and roughness are shown in Fig. 9.

Figure 9 shows that adding CH₄ to a H₂ plasma for QF etching does not significantly affect the resulting roughness nor the etching profile. Further characterization using TEM-EDX and ToF-SIMS did not suggest substantial improvement with CH₄ addition, so the focus has been oriented to N₂ addition. As shown in Fig. 9(b), adding 15% N₂ to H₂ already results in a strong nodes' size reduction. We have, thus, investigated higher N₂ dilution, as shown in Fig. 10 which illustrates the impact of N₂ dilution on the etching profile analyzed by Tilted SEM for etching conditions ranging from pure H₂ to 30% N₂ in a H₂-based plasma. As for all experiments, we maintained total gas flow rate constant in all plasma trials.

TABLE I. Process parameters effects on etch rates and resulting surface roughness.

	Reference H ₂ etch	Low pressure —50%	Low bias voltage —50%	Low temperature —42%
Etch rate (nm min ⁻¹)	375	405	273	303
Roughness RMS (nm)	33	19	42	14

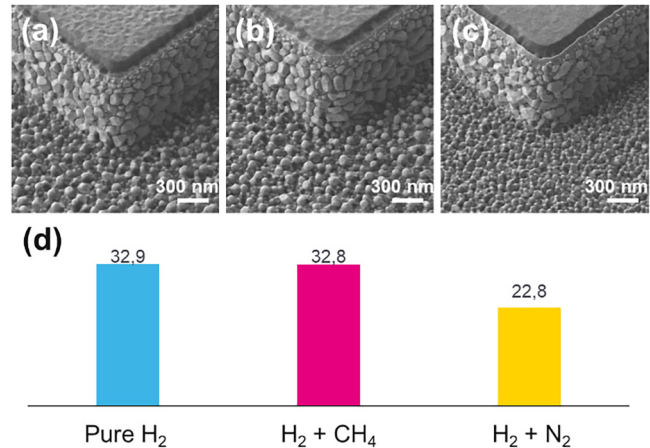


FIG. 9. SEM pictures [(a)–(c)] and RMS roughness measured through AFM inspection (d) of partially etched samples using H₂-based plasma including additional chemistries. (a) Pure H₂ chemistry, (b) H₂ + 10% CH₄, and (c) H₂ + 15% N₂. All scale bars are 300 nm.

By increasing the N₂ dilution into the H₂/N₂ gas mixture, both the surface and feature sidewalls become increasingly smoother. While the addition of 30% N₂ to a H₂ plasma reduces the etch rate, it also creates a more uniform etch front, which results in a smooth surface after a partial etch. This plasma chemistry appears promising and has been characterized by ToF-SIMS to further understand the role of N in the plasma/surface interaction (Fig. 11).

Figure 11(a) shows that the H density profile in the QF depends very strongly on the percentage of N₂ in the H₂/N₂ mixture. In pure H₂ and in H₂/N₂ with 15% N₂, H atoms diffuse deep into the QF (over 100 nm). As evidenced in Fig. 11(b), this is accompanied by a significant depletion of C–N bonds in the QF due to the etching of the QD ligands, facilitating H diffusion and resulting in Pb-rich dot fragments coalescence and roughness formation. Indeed, Figs. 11(c) and 11(d) show that the surface is significantly enriched in Pb and depleted in S under N-poor conditions. Consequently, in H-rich mixtures, the film is strongly damaged. By contrast, with 30% N₂ dilution [Fig. 11(a)], H diffusion in the QF is blocked since H is hardly detected beyond 5 nm from the surface. Simultaneously, the surface exhibits significant nitrogenation [Fig. 11(b)], showing that N atoms not only prevent etching of the CN bonds initially present in the QF but also lead to a nitrogenation of the carbon ligands and passivators. This 10–20 nm thick CN-rich surface layer apparently acts as a protective barrier, which prevents H diffusion in the QD film and, therefore, prevents the etching of the carbon-rich ligands and passivators by H atoms. As a result, Figs. 11(c) and 11(d) show that both the Pb and S density profiles are flat, indicating that N rich plasmas allows us to maintain the QF film initial stoichiometry and, thus, to achieve roughness-free etching since H reacts only with the extreme surface. We also underline that by contrast with Cl and Br atoms which are able to diffuse laterally several 100 s of

12 November 2024 14:43:05

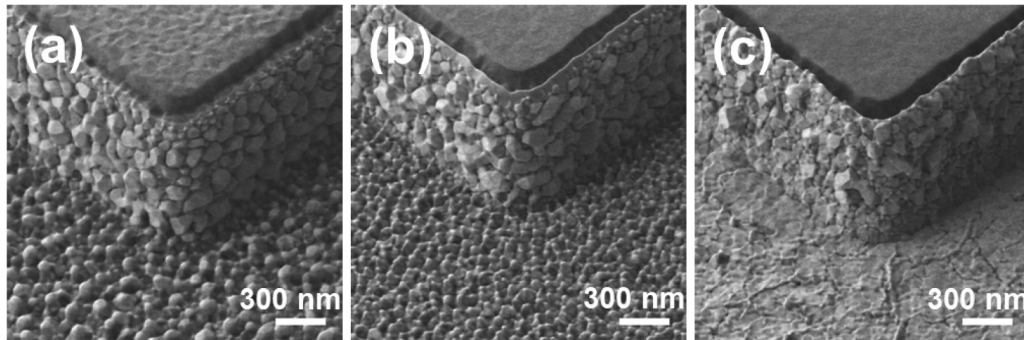


FIG. 10. Tilted SEM etching profiles from different N_2 dilutions in H_2/N_2 plasma. Corresponding dilutions and etch rates are (a) pure H_2 , 380 nm min^{-1} ; (b) $H_2 + 15\% N_2$, 190 nm min^{-1} ; and (c) $H_2 + 30\% N_2$, 200 nm min^{-1} . All scale bars are 300 nm.

nanometers deep underneath the mask, N atoms do not penetrate deeply in the QF: the 10–20 nm N rich layer that forms at the surface of the feature sidewall is negligibly thin compared to the micrometer-size of the final photodiode device and is, thus, not expected to affect its optical properties (especially since

nitrogen is already present in the QF film before etching). Therefore, H_2/N_2 with 30% N_2 plasma chemistry emerges as the most promising QF etching chemistry to date, facilitating anisotropic, selective, roughness-free, and H diffusion-free etching, thanks to the creation of a nitrogenated diffusion barrier.

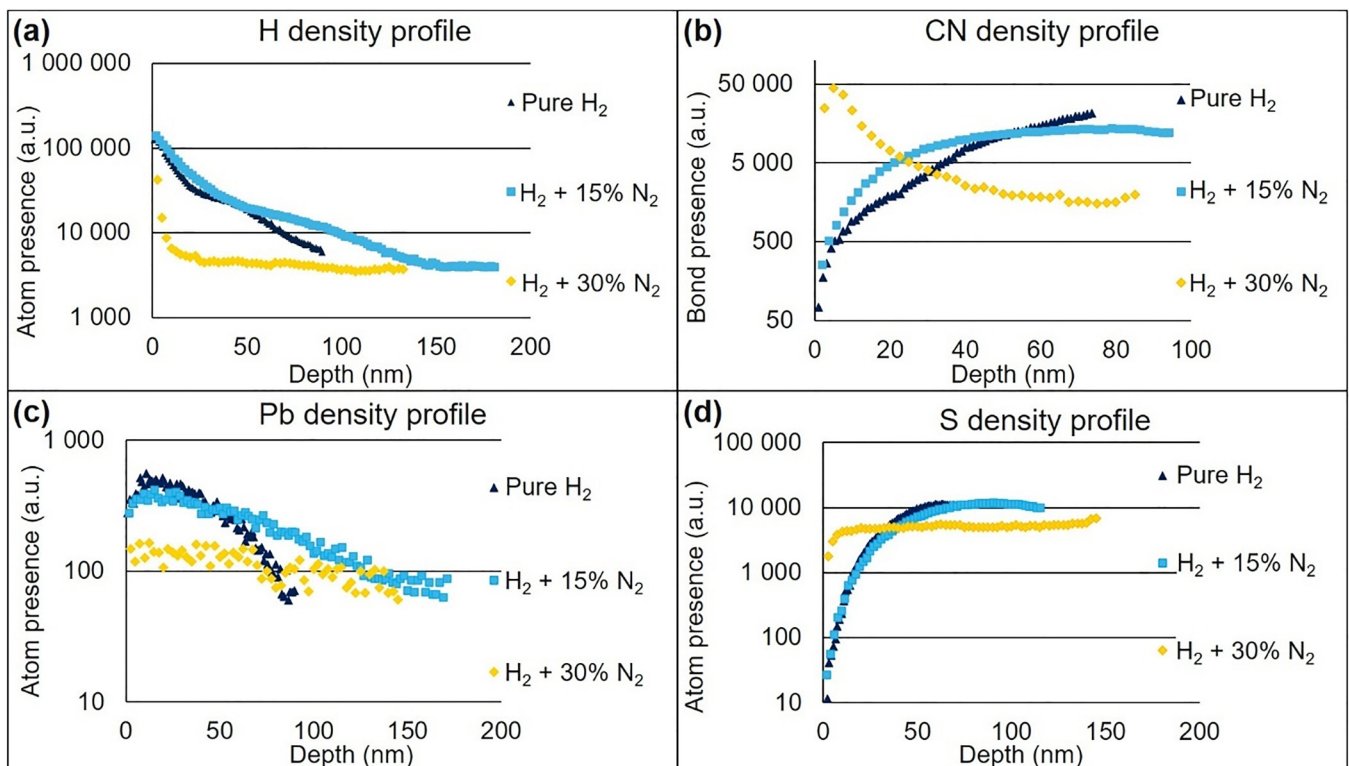


FIG. 11. Hydrogen (a), CN bonds (b), lead (c), and sulfur (d) density profiles obtained by ToF-SIMS measurements through remaining QF after partial etching using different dilutions of N_2 in H_2 -based plasmas.

12 November 2024 14:43:05

IV. SUMMARY AND CONCLUSIONS

We have investigated various plasma chemistries for the dry etching of a PbS QD thin film. Chlorine and bromine-based plasmas show etchant diffusion into the film, which threatens the integrity of the final device and prevents these chemistries from being suitable etchants. Hydrogen-based plasma, while leading to fast film etching, resulted in a rough surface. ToF-SIMS measurements identified the mechanisms creating this roughness: hydrogen atoms diffuse into the film, forming volatile species that preferentially etched sulfur and organic ligands. The removal of ligands and sulfur caused Pb dot fragments to coalesce, contributing to the roughness.

However, we found that the roughness can be significantly reduced by adding N₂ into the H₂ plasma. ToF-SIMS analysis suggested that nitrogen bonded with carbon from the organic ligands and passivators, creating a barrier against H diffusion. This dense CN bonds layer protected the ligands, preventing dot coalescence and resulting in a smooth etch front. Consequently, H₂/N₂ plasmas emerged as a favorable choice for patterning a PbS QD thin film.

ACKNOWLEDGMENTS

This work was partly supported by the French Renatech Network.

AUTHOR DECLARATIONS

Conflict of Interest

The authors have no conflicts to disclose.

Author Contributions

Nicolas Le Brun: Data curation (lead); Formal analysis (lead); Investigation (lead); Methodology (equal); Supervision (lead); Validation (lead); Visualization (lead); Writing – original draft (lead); Writing – review & editing (equal). **Gilles Cunge:** Conceptualization (lead); Formal analysis (equal); Funding acquisition (lead); Investigation (supporting); Methodology (supporting); Project administration (equal); Supervision (lead); Validation (equal); Writing – original draft (supporting); Writing – review & editing (lead). **Pascal Gouraud:** Conceptualization (lead); Data

curation (supporting); Formal analysis (equal); Funding acquisition (lead); Investigation (equal); Methodology (equal); Project administration (equal); Resources (supporting); Supervision (lead); Validation (equal); Writing – original draft (supporting); Writing – review & editing (supporting). **Camille Petit-Etienne:** Formal analysis (equal); Investigation (equal); Methodology (equal); Validation (equal); Writing – review & editing (equal). **Linda Parmigiani:** Data curation (equal); Formal analysis (equal); Investigation (equal); Methodology (equal); Validation (equal); Writing – review & editing (supporting). **Stéphane Allegret-Maret:** Conceptualization (equal); Investigation (equal); Project administration (equal); Resources (equal); Validation (equal); Writing – review & editing (supporting). **Denis Guiheux:** Data curation (equal); Formal analysis (supporting); Validation (supporting); Writing – review & editing (supporting). **Jonathan S. Steckel:** Conceptualization (lead); Project administration (lead); Resources (equal); Validation (supporting); Writing – review & editing (supporting).

DATA AVAILABILITY

The data that supports the findings of this study are available from the corresponding author upon reasonable request.

REFERENCES

- ¹T. Hirayama, in *IEEE Asian Solid-State Circuits Conference* (IEEE, New York, 2013), p. 5.
- ²Data taken from ASTM G-173-03 standard, see <https://www.pveducation.org/>.
- ³C. M. Herzinger, B. Johs, W. A. McGahan, J. A. Woollam, and W. Paulson, *J. Appl. Phys.* **83**, 3323 (1998).
- ⁴J. S. Steckel *et al.*, in *IEEE International Electron Devices Meeting (IEDM)* (IEEE, New York, 2021), p. 518.
- ⁵J. Yang, M. K. Choi, D. H. Kim, and T. Hyeon, *Adv. Mater.* **28**, 1176 (2016).
- ⁶D. Bera, L. Qian, T.-K. Tseng, and P. H. Holloway, *Materials* **3**, 2260 (2010).
- ⁷S. Ahn, W. Chen, and O. Vazquez-Mena, *Nanoscale Adv.* **3**, 6206 (2021).
- ⁸G. Yang and B. Weng, *Mater. Sci. Semicond. Process.* **124**, 105596 (2021).
- ⁹M. A. Foad, C. D. W. Wilkinson, C. Dunscomb, and R. H. Williams, *Appl. Phys. Lett.* **60**, 2531 (1992).
- ¹⁰G. Cunge, R. L. Inglebert, O. Joubert, L. Vallier, and N. Sadeghi, *J. Vac. Sci. Technol. B* **20**, 2137 (2002).
- ¹¹N. S. J. Braithwaite, J. P. Booth, and G. Cunge, *Plasma Sources Sci. Technol.* **5**, 677 (1996).

12 November 2024 14:43:05